Electronic Supplementary Material (ESI) for Nanoscale.
This journal is © The Royal Society of Chemistry 2019

Supporting Information

Extending pressure sensing range of porous polypyrrole with multiscale microstructures

Yunxia Li, Changjun Jiang and Weihua Han *

School of Physical Science and Technology, Lanzhou University, Lanzhou 730000, China.

*** Corresponding author.**

E-mail address: hanwh@lzu.edu.cn (Weihua Han)

1. Morphology and sensing characteristics of composite film

2. Flexibility of PPy/AgNWs/PDMS/PPy composite film

3. Material characterization

4. Characterization of the PPy film

5. Mechanical property

6. Compared with others microstructure

7. Stability of pressure sensor

8. Human motion detection

1. Morphology and sensing characteristics of composite film

The deposition time was arranged from 200s to 1000s, and the corresponding SEM images were shown in the Fig. S1a, 1b, 1c, 1d and 1e. Before 800s, the PPy deposited is insufficient to cover all the sponge surface which forms a discontinuous layer on the sponge. However, when the deposition time reaches 1000s, cracks appear on the surface due to excessive PPy deposition. Then, we conducted preliminary piezoresistive tests to samples with different deposition times and found that the relative current response was maximal when electrodeposited time is 800 s (Fig. S1f). In the following study, samples with depositing 800s PPy were selected for further study as a flexible pressure sensing material.

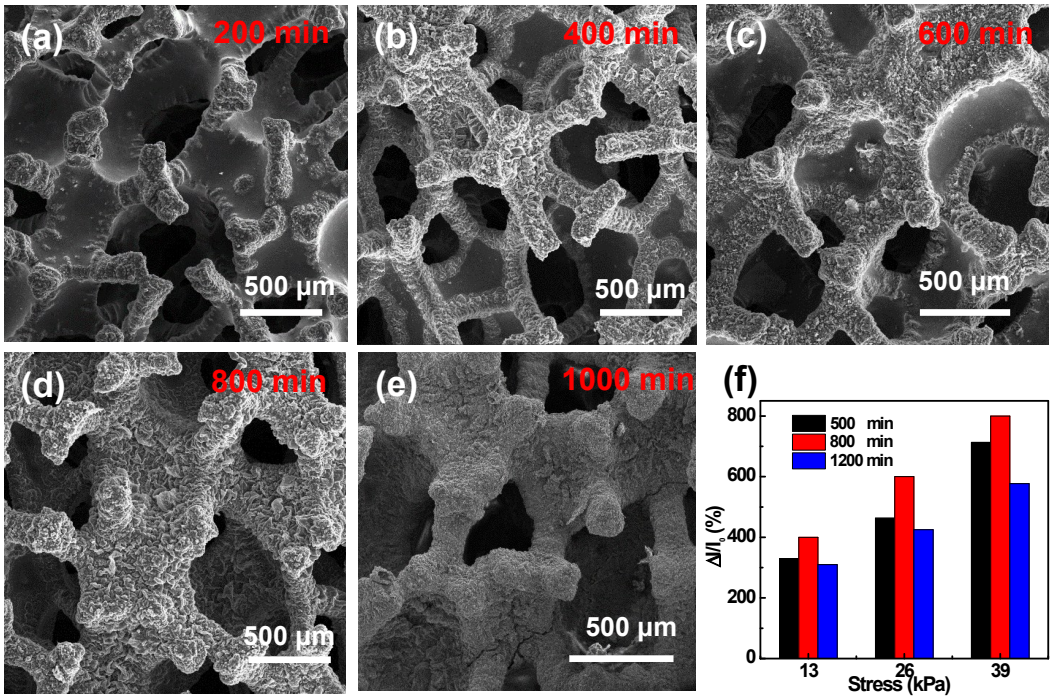

Fig. S1 SEM images of deposition PPy on the surface of AgNWs/PDMS/PPy with different time 200 min (a), 400 min (b), 600 min (c), 800 min (d) and 1000 min (e), and the comparison of sensing performance with different deposition time (f).

2. Flexibility of PPy/AgNWs/PDMS/PPy composite film

The free-standing 3D PPy/AgNWs/PDMS/PPy composite film is flexible and robust enough to sustain repeated compress to nearly 90% without fracture (Fig. S2a) and bending to nearly 180 degrees (Fig. S2b), exhibiting excellent mechanical stability, which benefits mainly from the unique interconnected backbones.

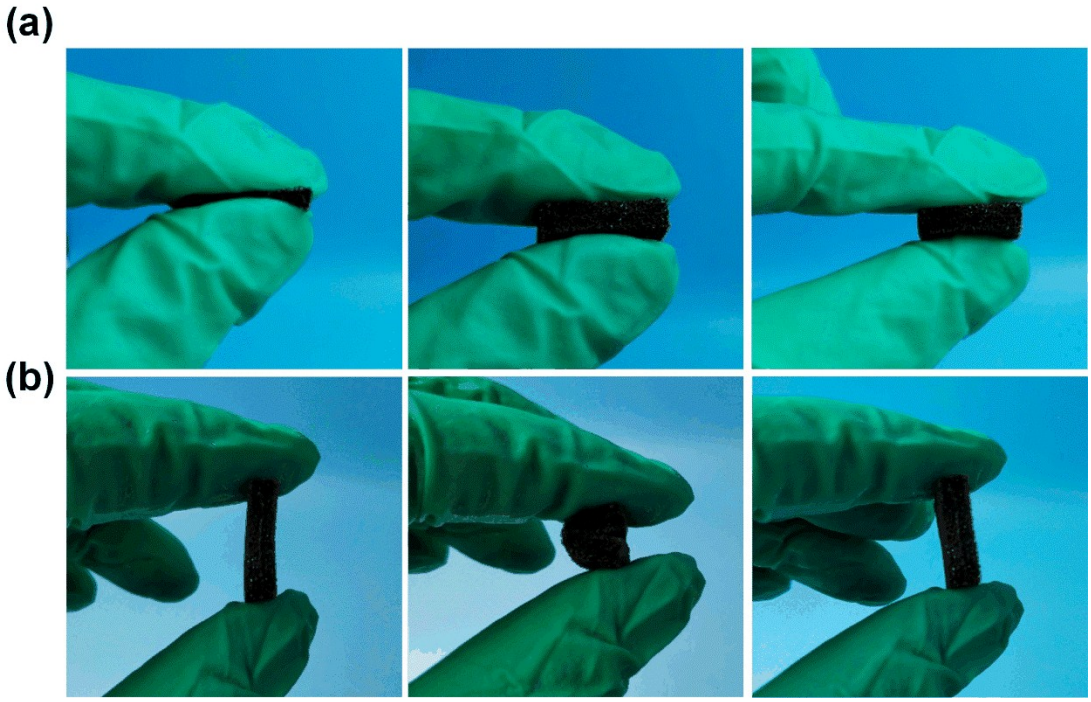

Fig. S2 Digital photographs of foam compressed (a) and bended (b) by fingers.

3. Material characterization

The morphology evolution from NF to the PPy/AgNWs/PDMS/PPy core-shell composites is illustrated in Fig. S3. A high magnification image (Fig. S3a) shows that the skeleton surface of the NF is extremely smooth. After PPy deposition, the skeleton surface became rough due to the existence of wrinkled PPy layer (Fig. S3b). The sample color turned into black as shown in the optical image in the inset of Fig. S3b, which

illustrates that PPy layer has completely and densely covered the skeleton surface of the NF. After being dried in an oven, a PDMS layer was coated on the skeleton of the PPy/NF to improve its stretchability as shown in the Fig. S3c and the skeleton surface became smooth. The sample color turned gray due to Ag NWs coverage illustrated in the inset of Fig. S3d, and the Ag NWs were interconnected with each other and formed a continuous conductive layer which completely wrapped the PDMS/PPy/NF skeleton (Fig. S3d). Another layer of PPy was electrodeposited on the surface of Ag NWs/PDMS/PPy/NF by using the Ag NWs/PDMS/PPy/NF as a working electrode. The skeleton surface was covered with wrinkled PPy again which has a rough surface (Fig. S3e). The surface color change back to black as indicated in the insert of Fig. S3e.

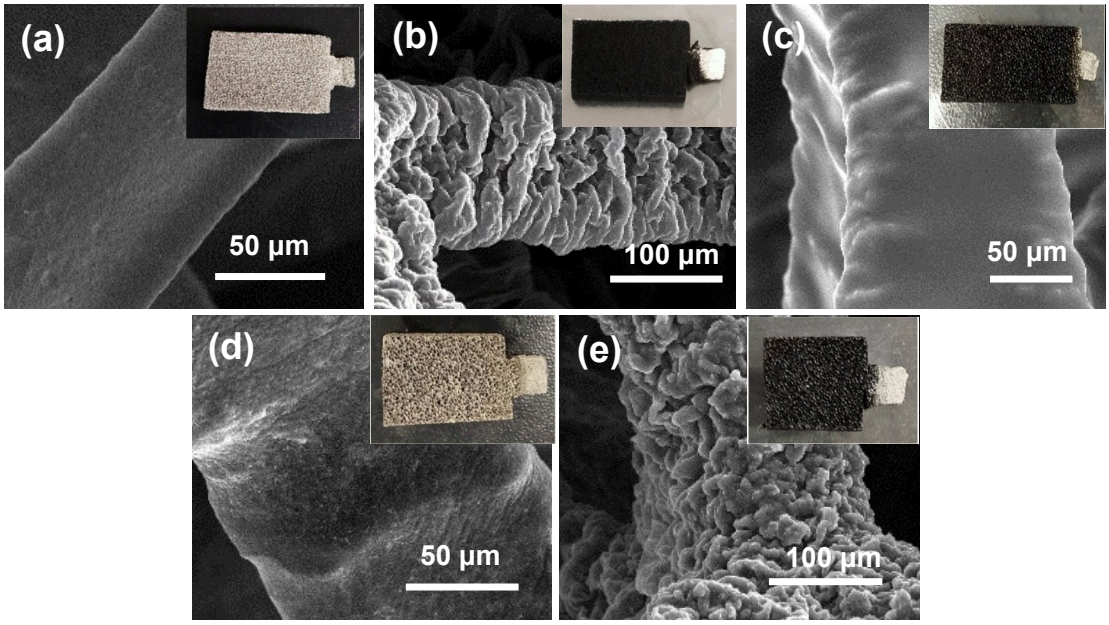

Fig. S3 Morphology evolution during the preparation of PPy/AgNWs/PDMS/PPy composite film. SEM images of cleaned, uncoated NF (a), electrodeposited PPy on NF with wrinkles and ripples (b), coating PDMS on PPy/NF (c), coating AgNW on PDMS/PPy/NF (d), electrodepositing PPy on AgNWs/PDMS/PPy/NF (e) and

corresponding their optical photos.

4. Characterization of the PPy film

It could be inferred that the foam was mainly consists of an amorphous solid PPy film, AgNWs and PDMS, since the broad XRD pattern around 25° and 11° were the characteristic peak of PPy and PDMS, respectively. The sharp peaks at 2θ values of 38.2°, 44.3°, 64.5°, 77.4° corresponding to (111), (200), (220) and (311), respectively, can be attributed to the pure phase of Ag (JCPDS file no. 04-0783), indicating the existence of Ag phase in the composites (Fig. S4a). In Fig. S4b, the strongest Raman peak at 1585 cm^{-1} is attributed to the mode of the conjugated C=C chain. The peaks at 1377, 1324, and 1242 cm^{-1} arise from the ring deformation. The double peaks around 932 and 966 cm^{-1} are related to the out-of-plane deformation of C-H, whereas the other double peaks located at 1053 cm^{-1} correspond to the N-H in-plane bending vibration. The strongest Raman peaks at 2964 and 2905 cm^{-1} are attributed to intense stretching vibrations of the methyl group of pure PDMS.

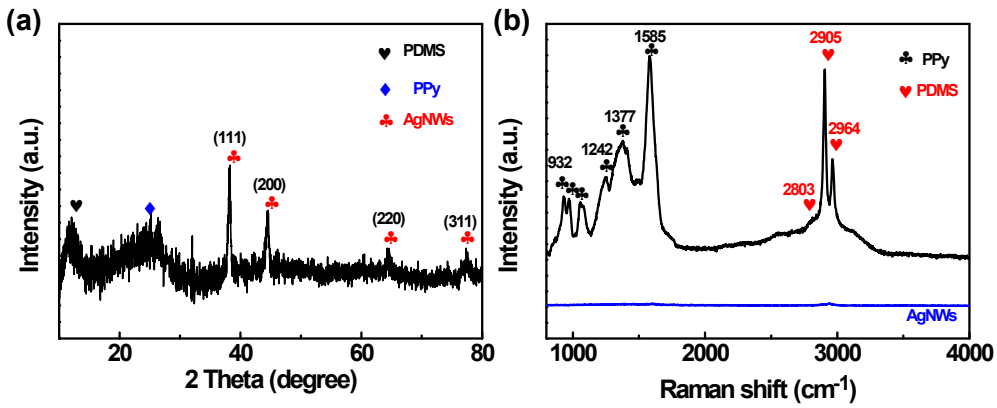

Fig. S4 XRD patterns (a) and Raman spectra (b) of PPy/AgNWs/PDMS/PPy composite film.

5. Mechanical property

Generally, good mechanical property is crucial for ideal piezoresistive sensor. Here, a series of compression tests were conducted at a compression rate of 1 mm/min to study the mechanical property of foam. The test platform was set up using a customized apparatus (Fig. S5a). The compressive stress σ versus stain ε curve for the obtained foam along the loading direction was shown in the Fig. S5b, three typical distinct stages were observed for the compressive stress-strain curves of foam. The linear elastic region for $\varepsilon<40\%$ within which the stress increased slowly and linearly. The reason for slowly increase in stress is due to the porosity of the foam. The plateau region for $40\%<\varepsilon<70\%$ within which the stress increased faster, the reason is the decreased porously of foam under strain. The densification region for $\varepsilon>70\%$ within which the stress increased sharply. Besides, it could be clearly seen that the stress could almost completely return to the initial point for each strain when the sponge was unloaded (Fig. S5c). Although we found hysteresis loops in loading-unloading cycles, indicating dissipations did not affect the shape recovery of the obtained foam. All these indicated the excellent elasticity without plastic deformation of composite film and these results were very important for the durability and reproductivity of ideal piezoresistive sensor.

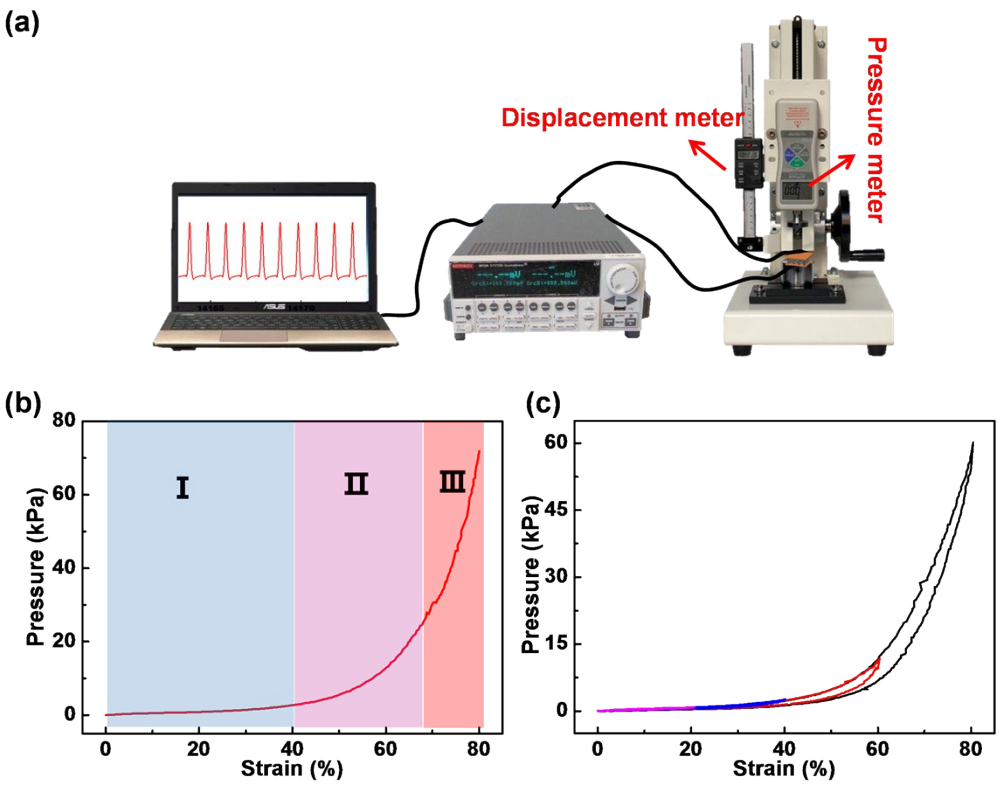

Fig. S5 Schematic of the experimental setup for mechanical property measurements (a). σ-ε curves of composite film (b). Different σ-ε cycle curves of PPy/AgNWs/PDMS/PPy with setting different strains of 40%, 60%, and 80%, respectively, at the compression speed of 1 mm/min (c).

6. Compared with others microstructure

In order to prove the superiority of multiscale microstructure, we compared it with other structures that PPy was only deposited on its outer or inner surfaces of hollow tube, respectively. And the final experimental results proved that the response of sensing material with multiscale microstructures under the pressure is higher than other structures as shown in the Fig. S6.

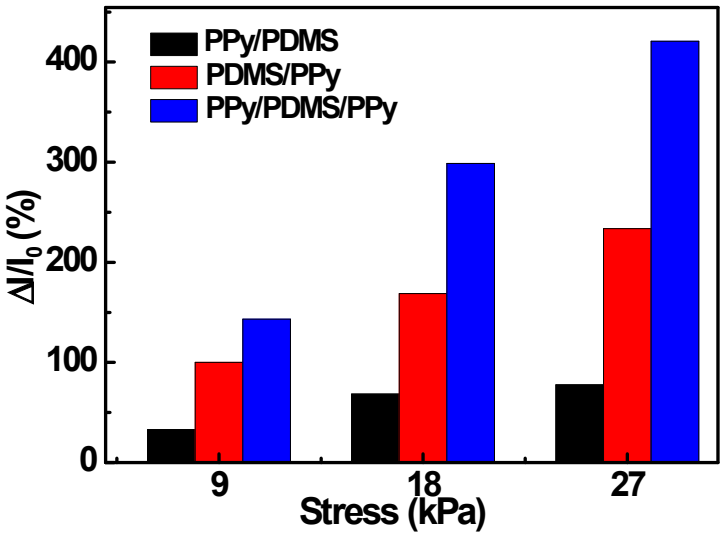

Fig. S6 Comparison of sensing performance among different microstructures.

7. Stability of pressure sensor

The durability and reliability are two most important factors of the pressure sensor for practical applications. The maximum and minimum of relative current change were almost the same during loading/unloading (Fig. S7a), respectively and the retention performance of maximum of relative current change after 16000 loading/unloading cycles under 10 kPa was shown in Fig. S7b. From the curve, the maximum was maintained more than 95% of its original value after 16000 loading/unloading cycles and the relative current change was basically the same at different frequencies (Fig. S7c), which indicated that the pressure sensor based on 3D composite films had a long working life and stability.

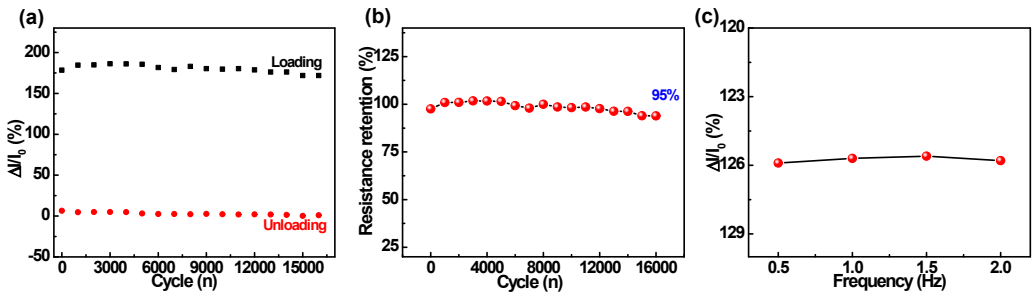

Fig. S7 Stability of the relative current change (a) and resistance retention (b) of PPy/AgNWs/PDMS/PPy composite film during the 16,000 loading–unloading cycles. (c) The current response to different frequencies at a fixed pressure.

8. Human motion detection

As shown in Fig. 7a and Fig. S8a, the wearable pressure sensor was affixed to the face and canthus to monitor the movement of facial muscles and eye in real time, and the responses were precisely recorded, the current patterns were almost the same with repeating the same action, indicating its outstanding ability in subtle human body motion detection. For the measurement of pulse signals, a characteristic peak of the typically single radial artery pulse waveform is shown in Fig. S8b and clearly contains three distinguishable peaks (P_1, P_2, and P_3) associated with an incident blood flow (P_1) and two reflected blood flows from the hand (P_2) and the lower body (P_3). The sensing behavior of finger bending was also observed, as shown in Fig. S8c. Obviously, current is enhanced by increasing the bending degree. To further prove the dependence of the current change on the bending angle of finger. The finger inclined at different angular positions are shown in the insert of Fig. S8c. It can be observed from the reported curves (Fig. S8c) that the sensor generates different responsive signals for different bending angles and the current change depends upon the bending degree. Therefore, the larger

the degree of bending, the higher the relative current variation.

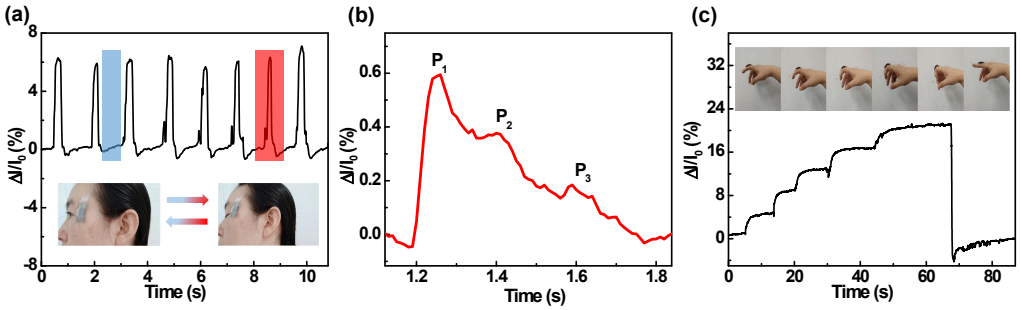

Fig. S8 Response curves of pressure sensor for the blinking (a), wrist pulse (b) and bending and release finger motions (c) under a fixed bias of 1 V.